

## Automated System for Optical Inspection of Defects in Resist-coated Non-patterned Wafer

A. Knápek, M. Drozd, M. Matějka, J. Chlumská, S. Král and V. Kolařík

*Institute of Scientific Instruments of the Czech Academy of Science, Královopolská 147,  
612 64 Brno, Czech Republic.*

Doi : <https://doi.org/10.47011/13.2.1>

---

*Received on: 08/08/2019;*

*Accepted on: 9/2/2020*

---

**Abstract:** Quality control of the resist coating on a silicon wafer is one of the major tasks prior to the exposition of patterns into the resist layer. Thus, the ability to inspect and identify the physical defect in the resist layer plays an important role. The absence of any unwanted defect in resist is an ultimate requirement for preparation of precise and functional micro- or nano-patterned surfaces. Currently used wafer inspection systems are mostly utilized in semiconductor or microelectronic industry to inspect non-patterned or patterned wafers (integrated circuits, photomasks, ... etc.) in order to achieve high yield production. Typically, they are based on acoustic micro-imaging, optical imaging or electron microscopy. This paper presents the design of a custom optical-based inspection device for small batch lithography production that allows scanning a wafer surface with an optical camera and by analyzing the captured images to determine the coordinates (X, Y), the size and the type of the defects in the resist layer. In addition, software responsible for driving the scanning device and for advanced image processing is presented.

**Keywords:** Optical inspection, Resist layer, Non-patterned wafer, Quality control.

### Introduction

Silicon wafer is a typical substrate that is used in lithography process for microfabrication of various types of devices. The quality of the silicon wafer determines the quality of a lithographic process, just as the quality of the resist-coated surface prior to the lithography step is very important in terms of the final functionality of the fabricated micro-device. Several papers have been published reporting optical properties of polymethyl methacrylate (PMMA) films [1, 2, 3].

Generally, there are two categories of wafer inspection methods: non-patterned and patterned [4, 5]. Non-patterned wafer inspection typically investigates defects on the unprocessed silicon wafer. On the other hand, patterned wafer

inspection is used for wafer control after the lithography process.

Industrial inspection devices used in semiconductor and chip manufacturing are based on two main technologies: optical and electron-beam [6, 7]. The optical inspection device typically uses laser, deep ultraviolet (DUV) or a broadband plasma light source to illuminate the wafer and acquire an optical image in the bright field or the dark field. In general, a principle of function, where a reflected laser beam carries information about a position, is illustrated in Fig. 1. The e-beam based inspection uses highly specified and automatized scanning electron microscopes that are typically used only for detailed inspection of patterned wafers [6].

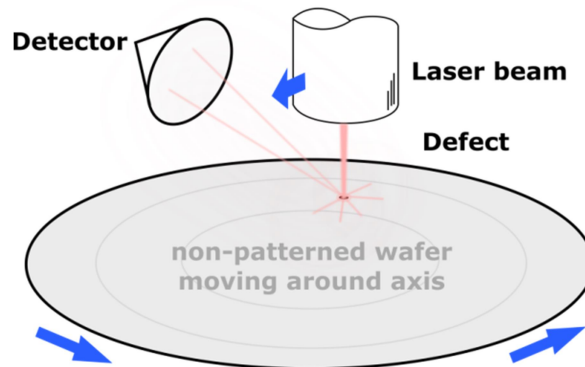


FIG. 1. Optically-based principle of defect inspection on a non-patterned wafer.

The devised approach is based on a motivation to develop an optical-based semi-automatic wafer inspection device that allows the inspection of a non-patterned [6] resist-coated wafer and would replace the current visual inspection of a wafer within the visible light microscope (VLM). Our primary aim is to find the position, the size and the type of the random defect at the layer of electron resist. That sort of evaluation is applied to a wafer surface by spin coating technique prior to its patterning by electron beam lithography (EBL).

Various types of defects are involved during the deposition of resist by spin-coating: dust contamination, micro-bubbles, bumps, craters,

comets, thickness inhomogeneity ... etc. [9, 10]. For the software, it is important to be able to identify not just the position of defects on the wafer, but also to estimate the type of defect, that may be considered as an essential feature, because not every type of defect can be equally problematic in the follow-up lithography process [9]. For example, a larger dust particle in or on the resist might cause a charging phenomenon, when the electron beam irradiates neighboring particles. Therefore, a charged dust particle can deflect the electron beam and reduce the dose received under and in the vicinity of the particle [11], as illustrated in Fig. 2.

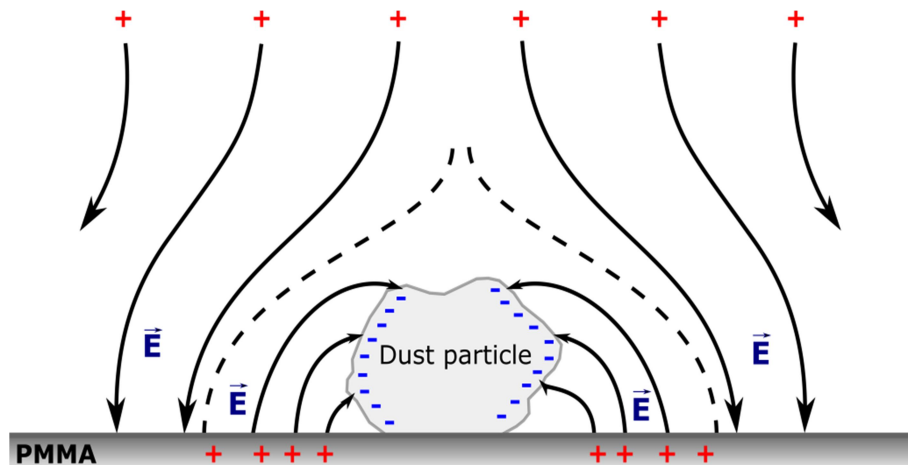


FIG. 2. Schematic of charging of a dust particle and the resulting defect in the EBL patterned wafer, with permission from Hitachi, Ltd., Tokyo, Japan [8].

It is critical to avoid patterning in the areas with particle contamination. Air bubbles might create holes in the resist after development. Comets can cause resist thickness inhomogeneity and thus an inadequate development of the recorded pattern.

## Defect Analysis

The preparation of PMMA resist layers on silicon wafers by spin-coating method is performed under laminar flow in order to lower the chance of a defect occurring in the prepared layer. The PMMA and xylene solvent are mixed together and, according to viscosity, are filtered through syringe filters (the porosity level is 0.45

$\mu\text{m}$  or  $5\ \mu\text{m}$ ). Subsequently, the resist is poured onto the silicon wafer which in this case forms an approx.  $2.5\ \mu\text{m}$  thick compact layer.

A variety of problems may occur during the coating process. In general, the above defects can be caused by impurities on the silicon wafer, such as dust particles, impurities or micro-bubbles in the resist mixture or by e.g. poor centering of the wafer on a spin coater. The parameters considered within the process of spin coating include rotation speed, acceleration, time and the application method of the liquid resist precursor.

The first class of defects is caused by impurities that stick to the resist layer during the deposition or during the baking process, as illustrated in Fig. 3. If a dust particle or fiber falls on the wafer during deposition, it becomes coated in the resist and forms a “comet” (a small thickness difference formed from the center of the particle to the edge of the wafer). Other possible particles are small resist flakes (i.e., dried resist) that stick to the layer and become permanently attached to the surface due to the baking process.

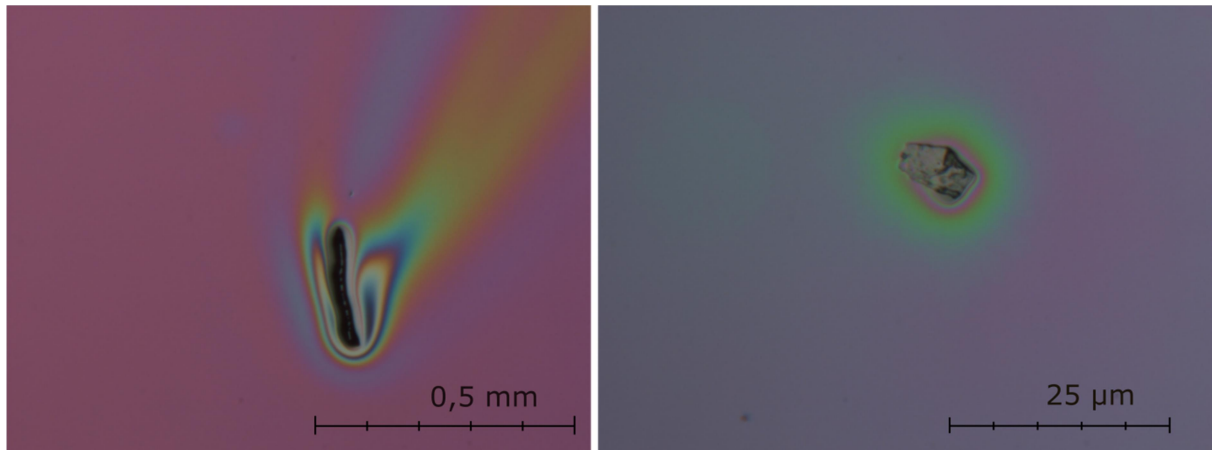


FIG. 3. Fiber creating a comet (left); a resist flake baked into the layer (right).

The second class of defects illustrated in Fig. 4 may occur randomly based on the processing technology. During the process of mixing of the resist and the solvent, air bubbles can form in the mixture. If a bubble is transferred on the wafer, it may form a defect called “micro-bubble”. It is a small spot (spherical shape) in the resist layer, where there is a huge thickness difference. It may cause problems during development (for example cracks in the resist layer around the spot). It can be prevented by degassing the mixture in the desiccator or really slow pouring of the resist mixture on the wafer. Another issue that may occur is related to inhomogeneity on a much bigger scale. For example, interference circles can be seen all over the wafer. The thickness difference is formed on a bigger

surface than in the case of micro-bubble defect. The exposed structure has afterwards different depths according to the location on the wafer. This type of defect can be caused by poor centering of the wafer on a spin coater, by an insufficiently levelled spin coater or by improper choice of the spin-coating parameters, as mentioned above. This type of defect cannot be seen using a microscope because of the small field of view. It can, however, be seen by the naked eye. Despite this kind of defect cannot be observed by the set-up, it has to be dealt with before the process of electron beam lithography and defected areas have to be avoided. This particular type of defect is further explained in the following paragraphs.

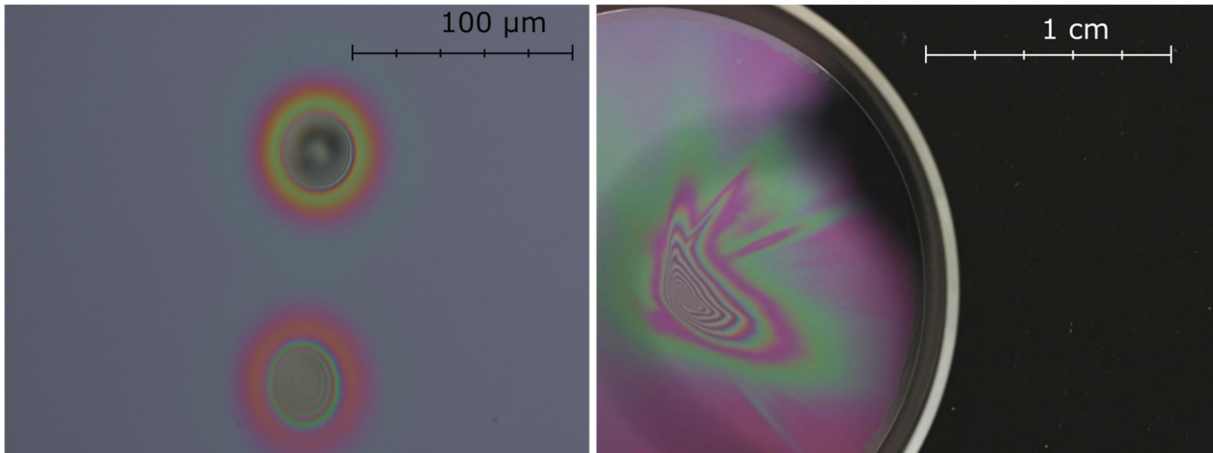


FIG. 4. Micro bubble (left), inhomogeneity all over the wafer (right). The left image was taken by VLM and the right one by a camera.

The interference effects, which can be seen in Figs. 3 and 4, are determined by the optical path length (OPL) through the thin PMMA film in a phenomenon called thin-film interference. Optical path length is the product of the geometric length  $d$  of the path of light through a system and the index of refraction  $n$  of the medium through which the light propagates, hence  $OPL = nd$ . Through this concept, a phase of the light can be determined by governing interference and diffraction of light as it propagates.

Recently, as was reported by Lalova [2], refractive index  $n$ , extinction coefficient  $k$  and thickness  $d$  of the spin-coated PMMA films deposited on a silicon wafer were determined by using minimization of a function. The function consists of the discrepancies between measured and calculated  $R$  spectra by means of multi-wavelength nonlinear curve fitting. The

refractive index was described using Sellmeier's equation in the following form:

$$n^2(\lambda) = 1 + \frac{A_1\lambda^2}{\lambda^2 - A_2^2}, \quad (1)$$

where  $A_1$  and  $A_2$  are the Sellmeier's coefficients. The dispersion of the extinction coefficient was described using the following exponential dependence [2]:

$$k = B_1 \exp\left(\frac{B_2}{\lambda}\right), \quad (2)$$

where  $B_1$  and  $B_2$  are dispersion coefficients. Based on Eqs. (1) and (2), it has been found out that the refractive index of the thin PMMA increases with the increase of the thickness following an exponential law of the type  $n = n_0 + A_1 (1 - \exp(-d/d_1))$ , where  $n_0$  is the initial value of the refractive index and  $A_1 = -0.9$  and  $d_1 = 31.91$  are parameters.

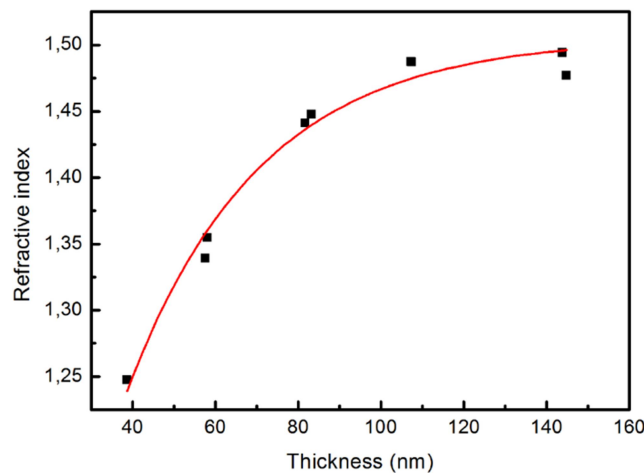


FIG. 5. Dependence of the refractive index on the thickness of thin spin-coated PMMA films at a wavelength of 600 nm, with permission from *Bulgarian Chemical Communications* [2].

Based on the dependence illustrated in Fig. 5, it has been concluded that the refractive index is thickness-dependent for values of  $d < 110$  nm. For thin films with thicknesses greater than 110 nm, the coating possess refractive index is close to that of the bulk [2].

## Measurement Set-Up

The measurement set-up illustrated in Fig. 6 consists of a table moving along the axis Y and a camera placed above the table which moves

along the axis X. The camera is based on a classical color CMOS sensor working at a resolution of 1.3 megapixels, allowing obtaining 15 screens per second with a resolution of 1280 x 1024 pixels over the USB 2.0 bus. The camera provides also a white LED lighting, whose intensity can be controlled manually. In order to reduce a distortion caused by the lens that may appear near the edges of the image, only the inner part of the image (approx. 70% of the original image) is used and further processed.

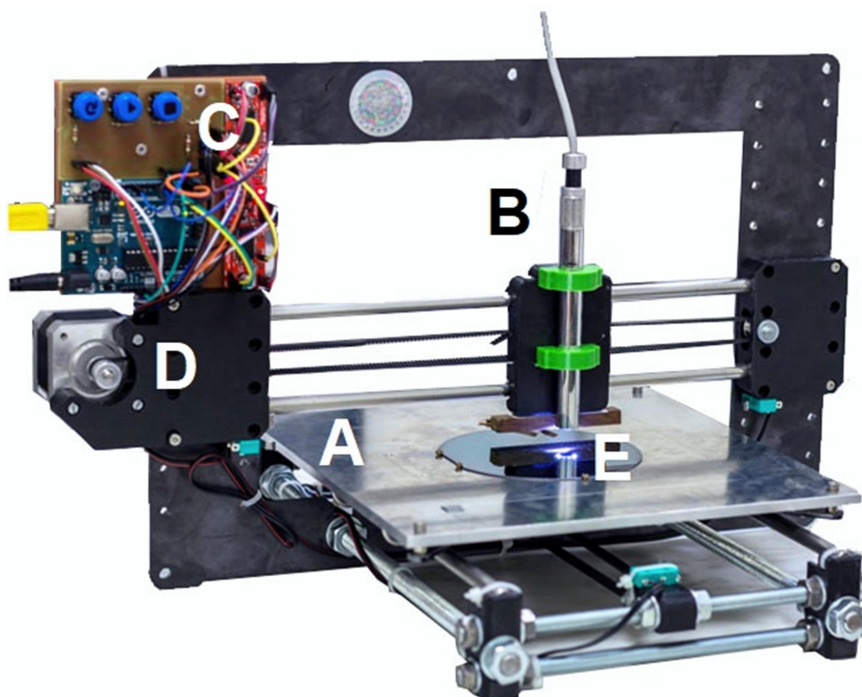


FIG. 6. Prototype of the measurement set-up scanning over a 4-inch wafer showing all the electronic and mechanical parts: (A) moving table, (B) camera on a moving holder, (C) Arduino board with buttons and stepper motor drivers, (D) stepper motor drive and (E) the evaluated 4-inch wafer.

The mechanical system was originally adapted from a 3D-printer-based platform with two precise stepper motors (see Figs. 6 and 7). The XY movement is based on the two stepper motors controlled through a microcontroller board Arduino UNO® based on the Microchip ATmega328P. The Arduino board contains its own program responsible for interpreting received commands from the WaferScan software (illustrated in Fig. 8, left), which includes driving of the movements. The board also generates a response when limit switches have reached the end of the track in one of the axes. The power supply to the motors is provided through two Easy Driver expansion boards. The whole system is powered using an external 12V DC power supply.

The main algorithm consists of a few simple steps that are implemented within an algorithm, whose flowchart is illustrated in Fig. 8 (right). In the beginning, the position of a calibration mark is located. The calibration mark is situated on a calibration sample, which is a silicon chip (1 cm<sup>2</sup>) with a cross-structure etched into the surface. This sample is placed on the stage table that contains also the evaluated wafer. After the position of the mark is read, a new coordinate system is set. This system of coordinates is then used for determining positions of any defect found during the scanning over the surface of the evaluated wafer. The flowchart illustrated in Fig. 8 (right) of the main scanning algorithm is implemented using Matlab graphic user interface (GUIDE®) and Matlab Instrumentation

toolbox®. Matlab instrumentation toolbox provides software means to communicate with all the components directly from the software by using text-based Standard Commands for Programmable Instruments (SCPI) command or *via* instrument drivers. The process follows a simple line scanning procedure, as it is known from any other scanning devices, which means that when an image is obtained, the camera

moves to another field of view until the whole surface is mapped. The implementation of post-processing uses advanced image processing and recognition techniques, whose description is outside of the scope of this paper; so, let us just simply conclude that the software returns precise coordinates and sizes of the defects found in the taken images.

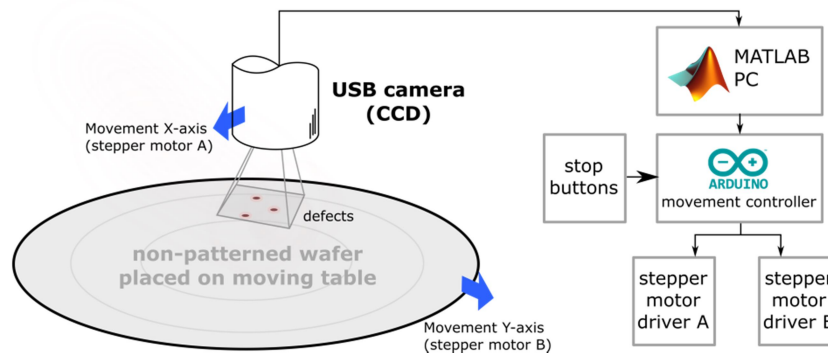


FIG. 7. Schematic illustration of the measurement set-up.

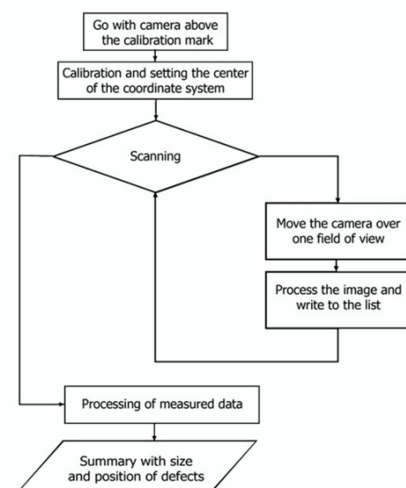
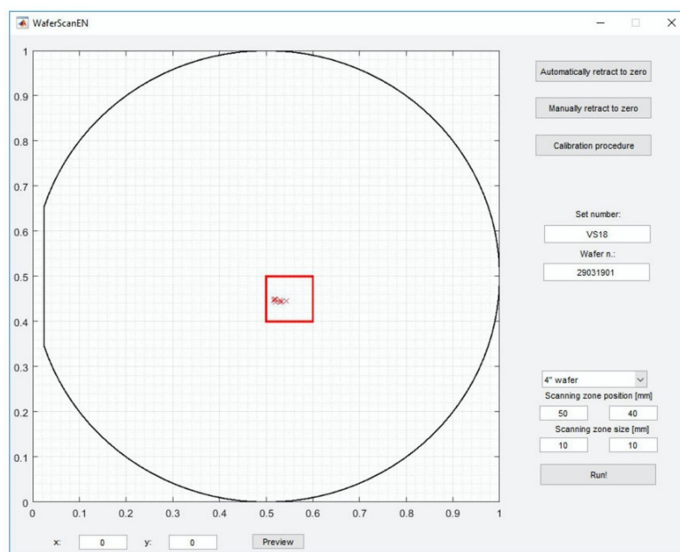


FIG. 8. The screen of the WaferScan software showing located defects in the red box (left); the flowchart of scanning algorithm schematically showing the implemented scanning procedure (right).

The WaferScan software (Fig. 8 left) allows running the initial calibration procedure both manually and automatically as well as precisely determining the area on the wafer to be scanned. On the background, the software saves a list of defects and their parameters as well as the particular images that are continually obtained for a possible further inspection. Using the saved images, it is possible to determine the size of the located defects.

## Results and Discussion

A comparison of two particular defects found is illustrated in Fig. 9, showing the output of our WaferScan system compared to the images obtained by manual inspection using a classical visible-light microscope. The map of defects shows the precise positions of the particular defects found.

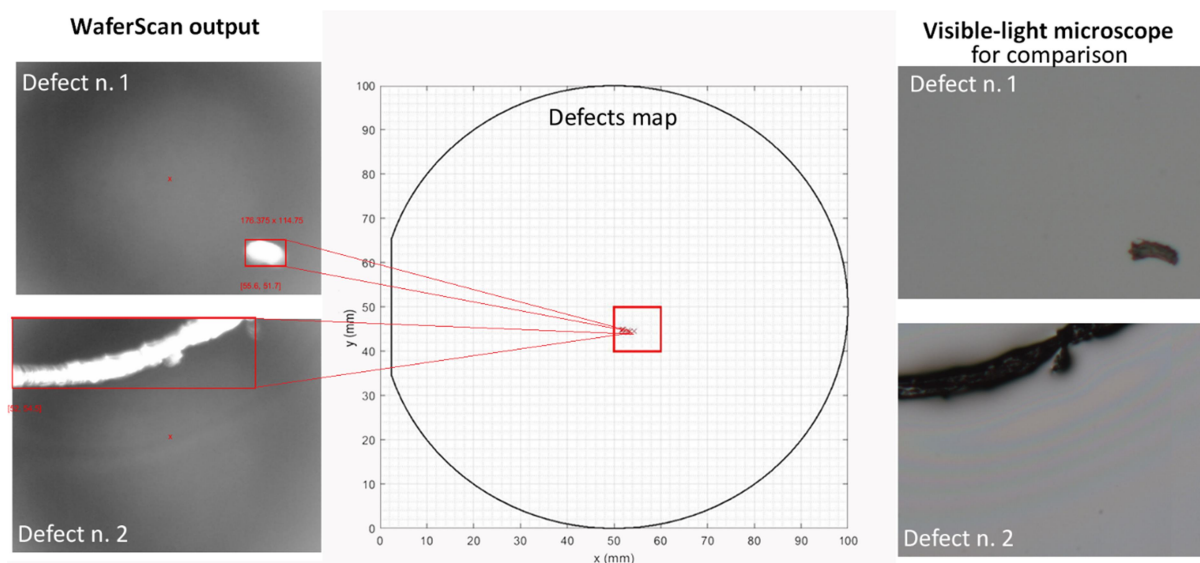


FIG. 9. Results provided for two selected defects (left top and above) within the scanning area (that is located within the red borders). On the right side, there are images from a visible-light microscope.

## Summary and Conclusions

This paper presents an important tool that has been developed to cover certain needs of complex research, which are connected with the development of large-sized micro-structure diffractive optical elements as well as sub-micron diffractive holography structures for industrial holography applications.

The devised set-up enables to scan a non-patterned wafer stepwise and to find defects as small as  $10\ \mu\text{m}$  by means of a precise CCD camera that scans the surface. Software, that is an essential part of the device, allows determining the size of a defect and its position on the wafer. This is the most significant benefit of this set-up, since the evaluation of a small series was in most cases done manually. Moreover, the accuracy of the process was increased and its error rate was decreased.

Further development will focus on precise characterization of particular defect types and automated distinction between defects, such as micro-bubbles, fiber or dust, in addition to revealing inhomogeneities of the resist layer on a smaller scale. The set-up will be further extended by addition of an automated focusing system that would make the process more precise. Among the other future goals, the set-up may be also extended to be used for patterned wafers and to implement White Light Reflectance Spectroscopy (WLRS).

## Acknowledgements

The research was supported by the Ministry of Industry and Trade of the Czech Republic, MPO-TRIO project FV10618. The research infrastructure was funded by the Czech Academy of Sciences (project RVO: 68081731).

## References

- [1] Norrman, K., Ghanbari-Siahkali, A. and Larsen, N.B., Annual Reports Section "C" (Physical Chemistry), 101 (2005) 174.
- [2] Lalova, A. and Todorov, R., Bulgarian Chemical Communications, 47 (2015) 29.
- [3] Hussein, A.S., Shinen, M.H. and Abdali, M.S., Journal of University of Babylon for Pure and Applied Sciences, 27 (4) (2019) 169.
- [4] Franssila, S., "Introduction to Micro-fabrication", (John Wiley & Sons, Ltd., 2006), pp.1-15 s. ISBN 0-470-85105-8.
- [5] Lapedus, M. "Inspecting Unpatterned Wafers", Semiconductor engineering, [online], 16 August 2018, Available at: <https://semiengineering.com/inspecting-unpatterned-wafers/>
- [6] Oberai, A. and Yuan, J.-S., Electronics, 6 (2017) 87.

- [7] Lapedus, M., "E-Beam vs. Optical Inspection", Semiconductor engineering [online], 16 July 2016, Available at: <https://semiengineering.com/e-beam-vs-optical-inspection/>
- [8] Yoda, H. et al., IEEE Transactions on Pattern Analysis and Machine Intelligence, 10 (1) (1988) 4.
- [9] Peerson, I., Thompson, G., DiBiase, T., Ashkenaz, S. and Pinto, R.H., Yield Management Solutions, 2 (3) (2000) 17.
- [10] Koch, Ch., Rinke, T.J., "Photolithography: Basic of Microstructuring", 1<sup>st</sup> Ed., (MicroChemicals, GmbH, 2017), pp.58-62 s. ISBN 978-3-9818782-1-9.